

Colloidal Silicon Quantum Dot-Based Cavity Light-Emitting Diodes with Narrowed and Tunable Electroluminescence

I Teng Cheong †, Josef Mock ‡, Maria Kallergi ‡, Elisabeth Groß §, Alkiviathes Meldrum ‖, Bernhard Rieger §, Markus Becherer ‡ and Jonathan G. C. Veinot* †*

† Department of Chemistry, University of Alberta, Edmonton, Alberta T6G 2G2, Canada

‡ Department of Electrical and Computer Engineering, Technical University of Munich, 85748 Garching, Germany

§ WACKER-Chair of Macromolecular Chemistry, Technical University of Munich, 85748 Garching, Germany

‖ Department of Physics, University of Alberta, Edmonton, Alberta T6G 2E1, Canada

ABSTRACT Luminescent colloidal silicon quantum dots (SiQDs) have been explored as alternatives to metal-based QDs for light-emitting diodes (LEDs) because of the abundance and biocompatibility of silicon. To date, the broad electroluminescence (EL) bandwidth (> 100 nm) and blue-shifting of EL at high applied voltages of SiQD-LEDs have been outstanding challenges that limited competitive spectral purity and device stability. Herein, we report the fabrication and testing of SiQD-LEDs that incorporate a Fabry-Pérot cavity that exhibit a narrow spectral linewidth as low as ca. 23 nm. The presented devices also provide spectral and visual stability from +4 V to +8 V, as well as spectral tunability.

1. Introduction

Colloidal quantum dots (QDs) are luminescent nanosized semiconductor particles that feature tunable optoelectronic properties. Following Brus' first report in 1980,¹ study of QDs is now a multidisciplinary research area that motivates vast technological development (e.g., photovoltaics,^{2, 3} sensors,^{4, 5} photocatalyst,⁶⁻⁸ etc.). Exploiting electroluminescence from QDs in light-emitting diodes (LEDs) has attracted interest for energy-efficient portable electronics because of the solution processibility, high color-purity, and stability.⁹⁻¹¹ An important limitation of commonly studied QD-LEDs is their reliance on non-earth abundant and/or toxic metals such as Cd, In, and Pb.¹²⁻¹⁵ Among the alternatives,¹⁶ Si is attractive because of its abundance, biocompatibility,¹⁷ compatibility with silicon-based electronics,¹⁸⁻²⁰ luminescent properties when formed as QDs, and its established/tailorable surface chemistry.²¹⁻²⁶

Electroluminescence (EL) of silicon-based nanomaterials (e.g., porous silicon,^{27, 28} Si nanocrystals in solid matrices²⁹⁻³¹) was first reported in the early 1990s and 2000s with low external quantum efficiencies (EQE) from 10^{-6} to 1 %. Of late, attention has shifted to colloidal silicon quantum dots (SiQDs) as potential active materials in hybrid organic light-emitting diodes (OLED) structures because of their promising EQE of up to 8.6 % for NIR EL and 6.2 % for red EL.¹⁸ Even with these improved metrics, the practical potential SiQD-LEDs remains limited by broad EL bandwidths with full-width-at-half-maximum (FWHM) that can approach 100 nm.^{19, 22, 32-41} Display applications require emission bandwidths of ≤ 50 nm to ensure appropriate spectral purity.⁴² Realizing this goal will undoubtedly contribute to the development of a variety of display technologies that exploit SiQDs.

Studies of SiQD photoluminescence (PL) show that narrow bandwidth luminescence can be achieved. In fact, under appropriate conditions individual SiQDs can exhibit a PL FWHM as narrow as 5 nm.^{43, 44} From this observation alone, one might be led to believe that narrow bandwidth emission, be it PL or EL, could be achieved by using well-defined materials of narrow size distributions. A variety of separation methods have been explored to narrow SiQD size distributions (e.g., size-selective precipitation⁴⁵ and density gradient ultracentrifugation⁴⁶) and by extension to reduce their PL FWHM. Surprisingly, the SiQDs “purified” in these ways still exhibited ensemble PL and EL FWHM of ca. 100 nm..^{34, 38} From these results, it is clear that alternative approaches toward narrowing SiQD EL must be explored if there is any hope of realizing practical SiQD-based display technologies.

Fabry–Pérot (FP) cavities are planar structures comprising a luminescent layer that is sandwiched between two reflective layers.⁴⁷ They present a promising approach toward narrowing and tuning the spectral linewidths of SiQDs in devices such as LEDs. In these FP cavity structures,

light reflected between the two mirrors interferes; the resulting standing wave consequently reduces the emission spectrum to only the resonant modes of the cavity and narrows the observed emission FWHM. Optical cavities have been used to narrow SiQD emissions.⁴⁸⁻⁵⁰ Amans et al., for example, have demonstrated a distributed Bragg reflector comprising a multilayer dielectric structure that could be used to filter and narrow SiQD PL achieving a FWHM of 13 nm in the 700 nm spectral region.⁴⁸ However, the fragility and complexity of this structure made it impractical for device applications. Recently, Zhang et al. presented an inorganic distributed feedback (DFB) LED of an oxide thin film containing SiQDs that exhibited an EL peak centered at ca. 638 nm with FWHM of ca. 33 nm.⁵¹ The emission spectrum however is ill-defined and the fabrication (i.e., electron-beam lithography) of the DFB grating is time consuming. Meldrum and co-workers instead demonstrated that sandwiching vapor deposited oxide-embedded Si nanocrystals (SiNCs) between two reflective metallic layers afforded a more straightforward approach toward PL narrowing achieving FWHM of ca. 10 nm for emissions spanning 480 to 1626 nm, however individual devices were not fabricated where the broad spectral range was achieved through a gradient thickness of silicon rich oxide.⁴⁹ Recently, we reported comparatively large area (i.e., 1 cm²) FP cavity structures prepared using solution processible SiQD-polymer hybrids and successfully narrowed the PL linewidth from more than 100 nm to ca. 9 nm.⁵² Our approach also enabled a broad color gamut and the realization of the first flexible emissive SiQD-based FP cavity. These advances in optically excited devices lay the groundwork for the present study and the fabrication of electrically driven self-emissive cavity-LEDs (cLED) based upon colloidal SiQD emitters.

2. Result and Discussion

The SiQDs used in the present cavity LED study were prepared using established procedures developed in our laboratories (Scheme 1a) that afford well-defined particle sizes and tailored surface chemistry suitable for material device incorporation/performance. We identified organolithium reagent (OLR)-mediated surface passivation (Scheme 1b) as the method of choice for introducing functionality to the surfaces of SiQDs because the resulting materials are solution-processable and resistant to oxidation.^{21, 26} In addition, OLR chemistry also introduces a comparatively low number of surface bonded molecules (vs. thermally-induced hydrosilylation functionalization)⁵³ through which carrier injection occurs more readily and facilitates dense packing of QDs; these factors are, in combination, expected to provide suitable film conductivity for SiQD cLEDs.²² For this reason, we chose to install a comparatively short surface group (i.e., hexyl; C₆ chain) in the presented SiQD LEDs.

The FTIR spectrum of Hex-SiQDs (Figure S1a) shows the expected C-H_x stretching (ca. 2922 cm⁻¹) and bending (ca. 1465 cm⁻¹) arising from surface bonded hexyl moieties. We also note Si-H_x related features (ca. 2077 cm⁻¹), as well as some limited surface oxidation appearing as Si-O stretching (ca. 1044 cm⁻¹). Thermogravimetric analysis (TGA) showed 30% weight loss in the temperature range of 300 to 400 °C (Figure S1b). These data taken together are all consistent with the limited degree of surface passivation afforded by OLR modification.

X-ray photoelectron (XP) spectra were acquired to probe the composition of, and element speciation within the Hex-SiQDs. The survey spectrum revealed the presence of only C (59.16 atomic %), Si (26.32 atomic %), O (14.52 atomic %), and traces of F arising from HF-etching (Figure S2a). The deconvoluted high-resolution Si 2p XP spectrum showed major Si (0) components at 99.3 eV indicating the elemental Si was preserved during functionalization (Figure S2b). Bright field transmission electron microscopy (TEM) imaging (Figure 1a) provided a mean

diameter of Hex-SiQDs of 2.78 ± 0.37 nm while PL spectroscopy of benzene dispersion provided an emission maximum of 726 nm with a FWHM of 144 nm (Figure 1b) and a quantum efficiency of 26%.

Scheme 1. Schematic representation of the synthesis of Hex-SiQDs used in the present investigation. (a) Preparation of H-SiQDs from thermally processed hydrogen silsesquioxane. (b) Functionalization of H-SiQDs upon reaction with 1-hexyllithium to yield Hex-SiQDs.

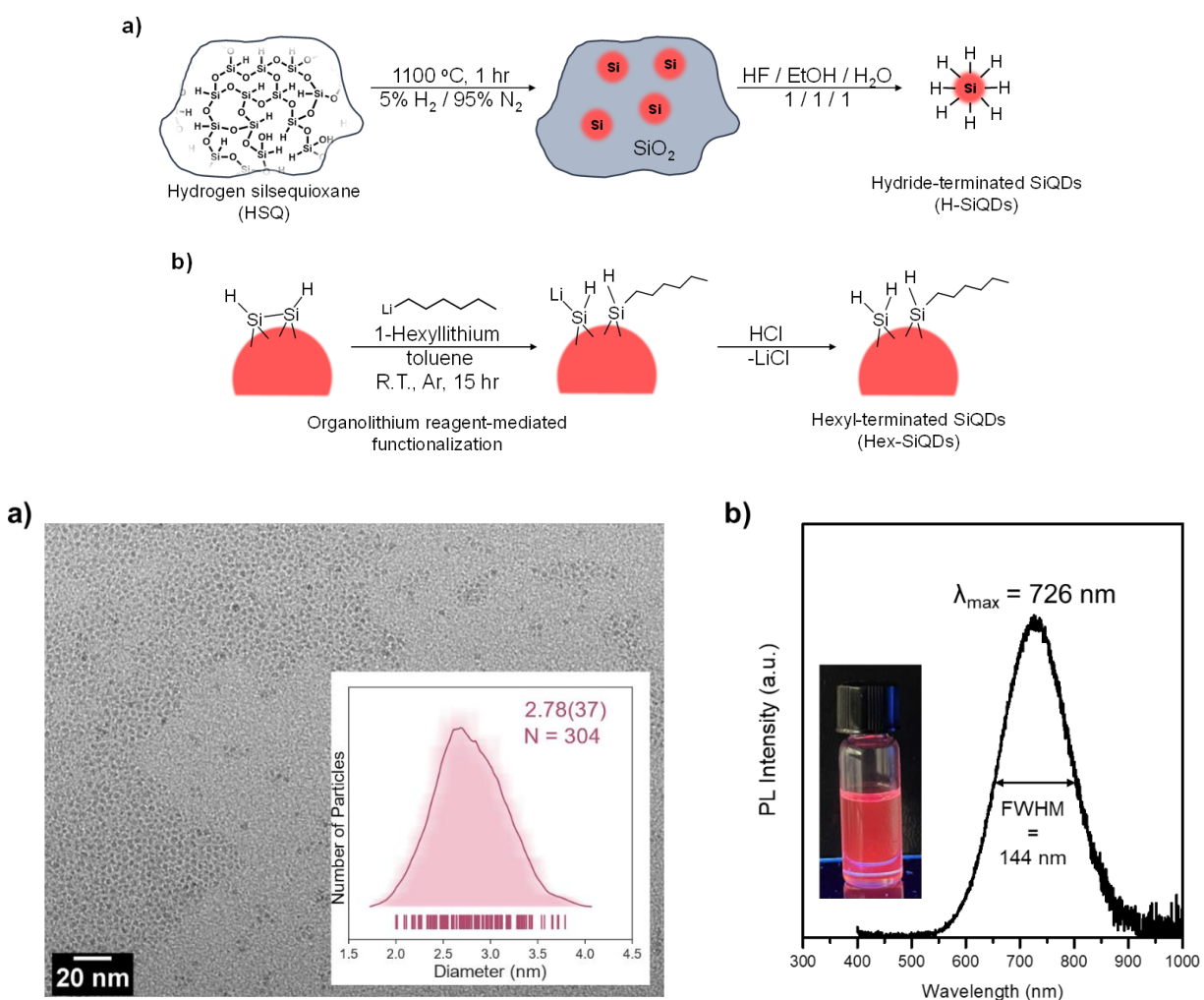


Figure 1. (a) BF-TEM image of Hex-SiQDs (Inset: Average shifted histogram presenting the size distribution of a representative sample of Hex-SiQDs.). (b) Photoluminescence spectrum ($\lambda_{\text{ex}} =$

365 nm) of Hex-SiQDs in benzene (Inset: A photograph of the solution upon exposure to a standard transilluminator UV lamp.).

With suitable Hex-SiQDs in hand, cLEDs were designed and fabricated with the goal of narrowing the electroluminescence FWHM of a SiQD-LEDs. The cLED structure incorporates a reflective mirror and SiO₂ layer into hybrid OLED stacks (Figure 2a-b). A thin, partially-reflective Ag layer (ca. 40 – 50 nm) and a transparent SiO₂ layer were first deposited on glass substrates via thermal and electron beam evaporation. The Ag layer (i.e., output coupler) exhibits a reflectance of 96.1 to 98.5% at 700 nm (vs. commercial silver mirror with a reflectivity of ca. 97%; Figure S3). Throughout the visible region that allows light to interfere within the cavity structure, leading to a narrowing of the spectral bandwidth while simultaneously allowing a fraction of the emission to escape. As part of the present investigation, the thickness of the SiO₂ layer was varied from 200 to 500 nm to define the optical pathlength of the cLED and tune the observed emission wavelengths. An indium tin oxide (ITO; work function = 4.92 eV; 10 nm; Figure S4a) anode was then deposited and coated with a layer of poly(3,4-ethylene-dioxythiophene) polystyrene sulfonate (PEDOT:PSS; 20 nm) to promote hole injection from the anode into the device. Poly(4-butylphenyldiphenylamine) (poly-TPD; 10 nm) was then deposited to ameliorate the injection barrier into the overlaying Hex-SiQDs. This was followed by the deposition of Hex-SiQDs (35 nm) and capped with a layer of zinc oxide (ZnO; 25 nm) that acts as a hole blocking and electron injection layer. Finally, an Ag cathode layer (100 nm) was deposited, which also serves as a mirror (99 % reflectance at 700 nm; Figure S3) that completes the FP cavity structure. Figure 2b shows an approximate energy level diagram for the present device.^{10, 21, 54, 55}

The resonance condition of the presented cLED structure is established when a photon emitted from the electroluminescent Hex-SiQD layer is reflected between the semitransparent Ag

output coupler and reflective Ag cathode. Resonant wavelengths (λ_m) of the cLED are given by Equation 1:

$$\lambda_m = \frac{2}{m} (\sum_i \eta_i d_i \cdot \cos\alpha + 2L_{pen,\alpha}) \quad (1)$$

where m is an integer defining the mode number, η_i and d_i are the refractive index and physical thickness of active layer i , α is the detection angle, and $L_{pen,\alpha}$ is the penetration depth in the metal mirrors. The total optical thickness is the summation

$$\sum_i \eta_i d_i = \eta_{SiO_2} d_{SiO_2} + \eta_{ITO} d_{ITO} + \eta_{PEDOT:PSS} d_{PEDOT:PSS} + \eta_{poly-TPD} d_{poly-TPD} + \eta_{SiQD} d_{SiQD} + \eta_{ZnO} d_{ZnO} \quad (2)$$

where all layers in between the two Ag mirrors are considered transmissive.

The refractive indices of each active layer were experimentally determined using ellipsometry and are provided in Figure S5. In addition to the active layers, each Ag mirror also induces a phase change upon the reflected photons. The penetration depth is estimated using Equation 3:

$$L_{pen,\alpha} = \frac{\lambda(\pi-\beta)}{4\pi} \quad (3)$$

where $\beta = \tan^{-1}[Im(r)/Re(r)]$ and r is the reflection coefficient obtained from the simulated complex index of refraction.⁵⁶ The cLED emission wavelength is tuned by varying the SiO₂ layer thickness while keeping all other layer thicknesses constant.

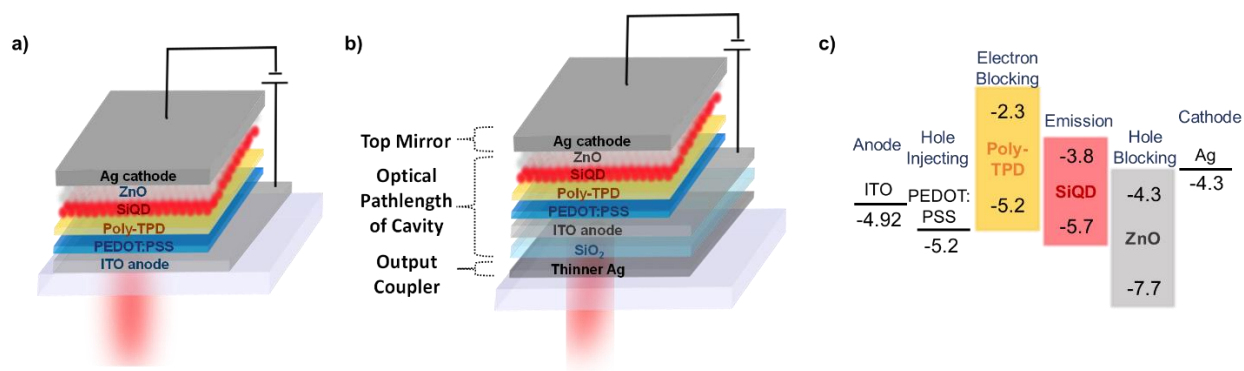


Figure 2. Schematic of the (a) cavity-free SiQD-LED, (b) SiQD-cLED device structure, and (c) associated energy level alignment. The thickness of the FP cavity can be tuned by defining the thickness of the SiO₂ layer.

To provide a baseline for the evaluation of presented cLED structures, a cavity-free SiQD-LED comprising the same stack structure (without the semitransparent Ag output coupler and SiO₂ layer) was fabricated and evaluated. As shown in Figure 3a, this device exhibited visibly detectable emission at a turn-on voltage of + 2 V with an emission maximum at 828 nm and a FWHM = ca. 113 nm at + 2 V. Figure S6a shows the absolute current density plotted against applied voltage (J-V plot) sweeping from - 4 to + 8 V for a standard SiQD-LED. No increase in passed current was observed under reverse bias conditions (i.e., $V < 0$ V) consistent with the device being “off”. For forward bias conditions, the J-V plot shows a clear current onset at + 2 V. The corresponding irradiance plot (Figure S6b) also shows an irradiance of $10 \mu\text{W cm}^{-2}$ suggesting a sufficient optical output could be achieved under this driving voltage to allow for detection. Prototype SiQD-LEDs investigated here showed external quantum efficiencies, EQE, approaching 1 % at a drive voltage of + 2 V (Figure S6c). We also noted that with increasing drive voltage from +2.0 to 5.0 V, the EL maximum blue-shifted from 828 to 735 nm and the spectral bandwidth broadened from 113 to 146 nm (Figure 3a, Table S1). These observations are commonly attributed to the inhomogeneous size distribution of the SiQDs, where the smaller QDs with larger band gaps can only be excited

with increased driving voltages.^{22,34} Of note, the EL spectrum obtained for a drive voltage of +4 V provided an emission maximum of ca. 743 nm with a FWHM of 146 nm that matched with the PL spectrum.

The cLED reflectance spectra were simulated to determine the appropriate SiO₂ thicknesses to provide cavities with resonant modes in the EL range of SiQDs from 650 to 900 nm (Figure S7). SiO₂ layers with thicknesses in the range of $d = 200$ to 350 nm were desirable for the present application. The model cavity structures with 350 nm thick SiO₂ layers provide an $m = 2$ resonance in the NIR region at 940 nm. The low resonance order is appropriate for films in the range of a few hundred nm thick; it moreover ensures a relatively large free spectral range (FSR), preventing multiple orders from occurring within the luminescence bandwidth. Decreasing the layer thickness to 200 nm blue-shifted this mode to approximately 700 nm. We limited our models to a maximum thickness of 500 nm because beyond this value the $m = 2$ emission would be out of the range of the SiQD EL spectrum.

Drawing on our cavity simulation results, we fabricated SiQD-cLEDs with 40 nm Ag output coupler and 350 nm thick SiO₂ layer (cLED-1). At an applied voltage of + 2.5 V, the optical cavity confined the SiQD EL into a dominant peak centered at 891 nm with a linewidth of ca. 24 nm (Figure 3b) – this is substantially narrower than the EL bandwidth obtained from a cavity-free SiQD-LED (i.e., FWHM = 113 nm; Figure 3a). The peak EL wavelength obtained for cLED-1 was at 891 nm, consistent with the $m = 2$ peak for a net optical thickness ~5% less than the expected value, which is quite good given the uncertainties associated with the deposition of multiple layers. The $m = 3$ mode occurred at ca. 602 nm which is at the short-wavelength edge of the non-cavity EL spectrum. Additional resonances corresponding to the $m = 3$ to $m = 6$ features were observed by reflectance spectroscopy (Figure S9, Table S2).

Looking to the device performance of cLED-1, the cavity-based device exhibits a higher apparent turn-on voltage than the equivalent cavity-free device (i.e., + 2.5 V vs. + 2.0 V). This can be attributed to the comparatively low transmittance of the Ag output coupler (ca. 2 % at 891 nm, Figure S3). Despite the necessity of a higher drive voltage, the cLED-1 emitted at a constant wavelength (whereas the equivalent cavity-free device spectrally shifted with increasing voltage). The principal EL maximum remained at *ca.* 891 nm for applied voltages in the range of + 2.5 to + 4 V with an average linewidth of ca. 25 nm and an average Q-factor of 36 ((Figure 3b; Table S3). We also note a minor EL emission peak corresponding to the $m = 3$ mode centered at 601 nm (FWHM = 24 nm, Q-Factor = 25) that emerged at higher voltages. The difference between the intensity of the two modes (i.e., 891 vs 601 nm) originates from the EL of SiQDs, as the cavity output traces the shape of the no-cavity spectrum. Under higher applied voltages, a shoulder emission was observed between the two modes. This leakage might be due to pinholes and inhomogeneity across the deposited layers as shown in the surface profile of the ITO layer (Figure S4b).

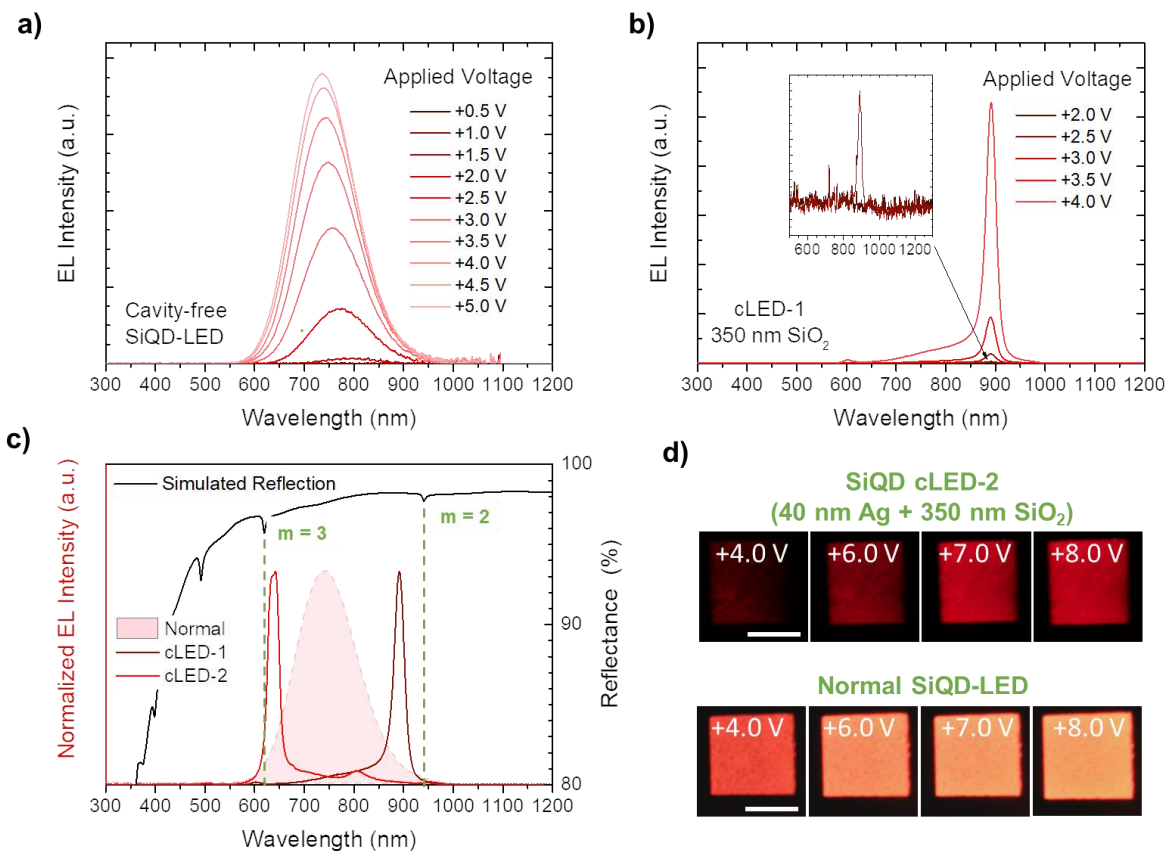


Figure 3. EL spectra of (a) cavity-free SiQD-LED and (b) cLED with 350 nm SiO₂ spacer (cLED-1) at different applied voltages. (c) Simulated reflectance spectrum (top) and EL spectra (bottom) of two different cLEDs with 350 nm SiO₂ spacer under +4 V. (d) Digital photographs comparing cavity-free LED and cLED-2 at different applied voltages. Inset scale bars are 2 mm.

The opportunity to couple SiQD EL to the modes of a device-embedded optical cavity to provide EL spectral tuning and bandwidth narrowing is further exemplified by cLED-2 – a device fabricated under the same conditions as cLED-1. Figure 3c shows the EL spectrum of cLED-2 which is dominated by an emission at 641 nm ($m = 3$) with a minor peak at 947 nm ($m = 2$). The observed resonant modes for cLED-2 are slightly red-shifted from the simulated spectrum suggesting the total cavity optical thickness is within ca. 4% of the targeted value (Figure S10).

As a result, the $m = 2$ peak is shifted beyond the SiQD EL envelope (i.e., $\lambda_{em} > 900$ nm) and the $m = 3$ peak is moved closer to the center of the SiQD EL spectrum. The $m = 3$ mode (i.e., $\lambda_{em} = 641$ nm) dominates the device response and the cLED-2 shows visible emission. It is immediately clear from visual inspection (Figure 3d top, Video S1) that the cLED-2 EL remained red (i.e., the wavelength did not change) with increasing voltage from + 4 to + 8 V. This is again in contrast to the spectral response of the cavity-free SiQD-LED for which EL shifted from red to orange (Figure 3d bottom Video S2).

The difference in the EL spectrum between cLED-1 and cLED-2, arising from minor variations in the cavity thickness, points to the opportunity for device spectral tuning through rational definition of the cavity optical pathlength. Figure 4a illustrates how defining the SiO₂ thickness in the range of 350 to 200 nm allows tuning of the emission maximum from near infrared (NIR) to red/orange. These cLEDs emitted at 776, 728, and 668 nm for nominal SiO₂ layer thicknesses of 300, 250, and 200 nm, respectively. As expected, the reflectance spectra of these cLED cavities also showed an increasing free spectral range (FSR) with decreasing thicknesses (Figure S11). The EL bandwidths of thinner devices (i.e., SiO₂ thicknesses of 350 to 200) are in the range of 43 to 105 nm, exhibiting Q-factors of only 7 to 15 (Table S3). This can be attributed to inconsistencies in the surface morphologies of the layers across different samples. When the SiO₂ layer thickness was increased to 500 nm, observed principal EL was centered at 691 nm with a FWHM of 31 nm and a Q-factor of ca. 23 (Figure 4b). This device was found to have more uniform microscopic morphology, as revealed by the three-dimensional atomic force microscopic (AFM) profile in Figure 5a. The two-dimensional AFM profiles in Figure 5b show that the root mean square (RMS) surface roughness of the full stack cLED is 2.45 nm where the roughness of each layer is between 0.36 to 2.20 nm.

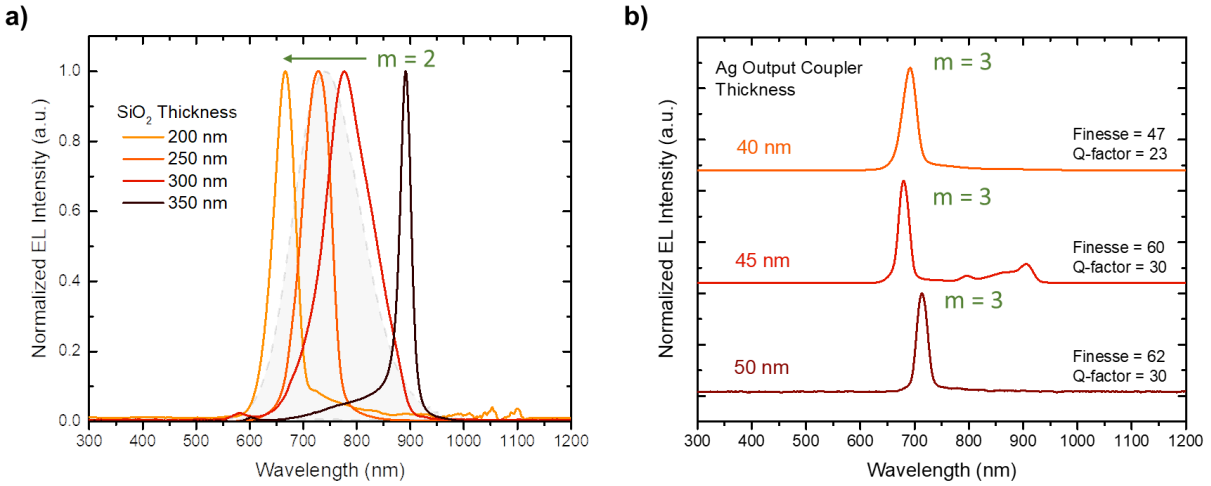


Figure 4. (a) EL spectra of SiQD-cLEDs with different SiO₂ thicknesses showing tunable emission ranging from reddish orange to NIR. The grey spectrum corresponds to the EL of the control LED. (b) EL spectra of cLEDs with different Ag output coupler thickness; all devices were deposited with 500 nm SiO₂.

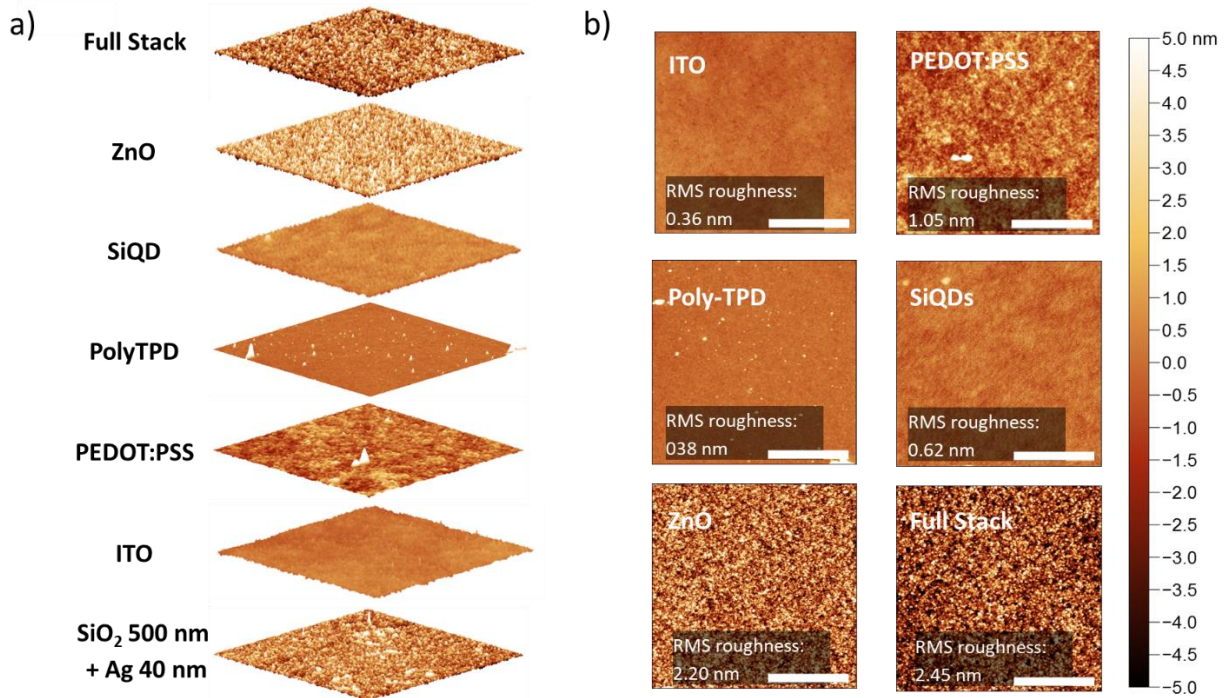


Figure 5. Smooth surface profile of SiQD-cLED with 40 nm Ag and 500 nm SiO₂ spacer revealed by (a) three-dimensional and (b) two-dimensional AFM images. Inset scale bars are 2 μ m.

In general, more reflective mirrors are expected to narrow the emission spectrum. Therefore, SiQD-cLEDs with 40, 45, and 50 nm thick Ag output couplers were fabricated and tested. As discussed previously (Figure S3), a 40-nm-thick Ag output coupler has a reflectance of 96.1 % at 700 nm, increasing to 97.8 and 98.5% when the thickness is increased to 45 and 50 nm, respectively. With the same SiO₂ spacer thickness (i.e., 500 nm), the cLEDs exhibited principal $m = 3$ EL emission centered at ca. 695 ± 18 nm (Figure 4b). The minor spectral leakages (i.e., shoulder emission) could be due to film inhomogeneity as evidenced by the reflectance spectra (Figure S11a, Table S4). The emission bandwidths of the devices with 45 and 50 nm thick Ag output couplers (i.e., 45-cLED and 50-cLED) were ca. 24 % narrower (FWHM = ca. 23 and 24 nm) as compared to the cLED with 40 nm Ag (40-cLED, FWHM = ca. 31 nm). Simulations showed a similar relative change in the cavity Q-factor (Figure S11b, Table S5-6). The lower Q-factors in the experiment are likely caused by surface roughness as apparent in the AFM images (Figure 5).

When the detection angle was changed from normal incidence to 15° off normal, the emission bandwidth of another 50-cLED remained ca. 30 nm (Figure S12). The complementary angle-dependent measurement also revealed a narrow cone of cLED emission of +15° from the surface normal with a slight blue-shift (ca. 10 nm), which is congruent with the optical characteristic of a FP cavity.⁴⁷ This directional emission could potentially reduce spectral overlap associated with nearby pixels in display device configurations.⁵⁵ In comparison, the broad, weak background emission showed no angular dependence.

Similar to the SiQD-cLED with a 40 nm thick Ag mirror discussed in Figure 3c, the 50-cLED exhibited stable emission under different applied voltages (i.e., + 3.5 to + 5 V) with a center

wavelength around ca. 714 nm and a Q-factor of ca. 30 (Figure S13, Table S5). Despite the impressive advances compared to the non-cavity device, the 50-cLED exhibited higher current densities up to + 4 V and a higher turn-on voltage of + 3.5 V as shown in the J-V and irradiance plot (Figure S14a); the maximum irradiance of the 50-cLEDs was only around $60 \mu\text{W cm}^{-2}$ with an EQE of ca. 0.004% (Figure S14 b-c). In contrast to the normal (no cavity) LED, the cLED EQE remained constant after an initial increase for voltages up to + 8 V. Again, the reduced efficiency of the cLED could be attributed to low transmittance at visible wavelengths, as well as inhomogeneities of the layered structure.

Incorporation of SiQDs with brighter emission via different functionalization method⁵⁷ or output coupler with higher transmittance (e.g., WO_3/W etc.)^{58, 59} would likely improve the output intensity and EQE of the cLEDs. Furthermore, optimizing the fabrication procedure and the device structure^{20, 39} to improve the stability, spectral response, and reproducibility of the cLEDs are subjects of ongoing investigations. Despite these issues, this work demonstrated the first example of an SiQD microcavity-based hybrid LED that exhibited defined emission and spectral tunability.

3. Conclusions

We successfully narrowed the broad SiQD electroluminescence linewidth from over 100 nm to as narrow as ca. 23 nm by incorporating hybrid SiQD-LEDs in a Fabry–Pérot cavity. The cavity-LEDs demonstrated excellent spectral and visual stability over a range of applied voltages. Using the same SiQDs, tuning the LED emission from visible (red-orange) to NIR was achieved by varying the thickness of the SiO_2 spacer inside the structure. The emission linewidth was also tunable via different Ag thicknesses. These SiQD cavity-LEDs offer a narrower emission spectrum, improved wavelength stability, and facile spectral tunability. This straightforward configuration

demonstrates the potential to develop spectrally pure SiQD LEDs and represents a step toward future heavy-metal free SiQD-based light-emitting technologies.

4. Experimental

Materials Hydrofluoric (Electronic grade, 48–50%) and sulfuric (reagent grade, 95–98%) acids were purchased from Fisher Scientific and Caledon Laboratory Chemicals, respectively. Fuming sulfuric acid (reagent grade, 20% free SO₃ bases), trichlorosilane (99%), toluene (HPLC grade), methanol (reagent grade), ethanol (reagent grade), isopropanol (reagent grade), *n*-hexyllithium (2.3 M in hexane), 1,2-dichlorobenzene were purchased from Sigma Aldrich. Dry solvents were obtained from a Pure-Solv purification system with N₂ as the operating gas. PEDOT:PSS (Al 4038) solution, poly-TPD, and ZnO nanoparticles (5.6% w/v in IPA) were purchased from Ossila, Solaris Chem, and Infinity PV. All reagents and solvents were used as received unless otherwise specified.

Preparation of Hydrogen Silsesquioxane (HSQ). HSQ was synthesized adapting a literature procedure⁵⁷. Briefly, a mixture of concentrated (15 mL) and fuming (7 mL) sulfuric acid was diluted with dry toluene (45 mL) under an Ar atmosphere. A solution of dry toluene (110 mL) and trichlorosilane (16 mL) was prepared and then added dropwise to the sulfuric acid mixture over a few hours. The toluene layer was isolated and washed with aqueous sulfuric acid solution. After the organic layer was dried over MgSO₄ (neutralized with CaCO₃ overnight), the solvent was reduced using a rotary evaporator and then evaporated in vacuo to yield a white solid that was stored under vacuum until use.

Preparation of the H-SiQDs. A modified literature procedure was used to prepare H-SiQDs.⁵⁸ Briefly, an appropriate amount of HSQ (e.g., 2 g) was annealed in a standard tube furnace under flowing 5% H₂/95% N₂ at 1100 °C. This procedure yielded oxide composite containing Si

nanodomains. The resulting composite was ground using an agate mortar and pestle and shaken in ethanol within a wrist action shaker with high purity glass beads for 16 h. The resulting powder was obtained through vacuum filtration and dried overnight. The composite (300 mg) then was etched using a 1:1:1 solution of ethanol:deionized water:HF (3 mL : 3 mL : 3mL) to liberate the H-SiQDs. After 30 to 60min, the solution turned pale orange. The SiQDs were then extracted from the aqueous layer using toluene and isolated by centrifugation (3000 rpm for 10 min or 9000 rpm for 4 min). Extracted particles were redispersed in 5 mL dry toluene and centrifuge again to remove residual etchant. The nanoparticle pellet was used immediately after the purification.

Preparation of the Hexyl-SiQDs using OLR. Functionalization of hydride-terminated SiQDs with organolithium reagent was adapted from previous literature procedure. Briefly, H-SiQDs obtained after liberation were immediately redispersed in dry toluene (2 mL) and transferred to a oven-dried Schlenk flask. The dispersion was degassed with three freeze-pump-thaw cycles and backfilled with argon. n-Hexyllithium solution (~ 0.4 mmol, ~ 0.2 mL) was immediately added to the reaction mixture. A dark brown solution was obtained after stirring at room temperature for 16 h. A 1 : 1 methanol : ethanol mixture (12 mL) acidified with HCl (~ 0.2 mL, ~12 drops) was prepared in Teflon tubes to terminate the reaction. Subsequently, the functionalize particles was precipitated by dropwise adding the reaction mixture into the quenching solution. The particles were then isolated after centrifugation (9000 rpm, 10 min). The solid pellet was resuspended in a minimum amount of toluene (~ 0.5 mL) and precipitate with the alcoholic mixture again. The purification cycle was conducted once more. The purified SiQDs were redispersed in benzene (2 mL), filtered through a 0.20 μm PTFE syringe filter, and freeze-dried. The hexyl-SiQD powder was ready to use or transferred into the glovebox for storage.

SiQD LED Fabrication. Normal SiQD LEDs with were fabricated on prepatterned ITO (15 Ω/\square , 120 nm) glass substrates following Mock, *et al.*'s work.²² Poly-TPD solution (5 mg mL⁻¹ in dry dichlorobenzene) and diluted ZnO nanoparticles solution (1:3 weight ratio in dry isopropanol) were prepared a day ahead. All substrates were cleaned with detergent water, acetone, and isopropanol sonication baths for 10 min at 60 °C, in the above order. Residue IPA on the substrates were removed with pressurized N₂ and further dried on a hot plate at 140 °C for 2 min. To improve the wettability of the PEDOT:PSS aqueous solution, the PEDOT:PSS stock was diluted with isopropanol (3:1 weight ratio) and filtered through a 0.45 μm regenerated cellulose filter right before deposition. The PEDOT:PSS layers (20 nm) were fabricated by static spin-coating ($\sim 70 \mu\text{L}$, ~ 3000 rpm, 30 sec) and annealed for 10 min at 140 °C in ambient condition. Afterwards, the substrates were transferred into a nitrogen-filled glovebox for further processing. The poly-TPD layers (10 nm) were then fabricated by static spin-coating ($\sim 70 \mu\text{L}$, ~ 4000 rpm, 30 sec). A freshly prepared SiQD solution (15 mg mL⁻¹ in dry toluene) and the diluted ZnO nanoparticles solution were freshly prepared and passed through 0.2 μm PTFE syringe filters. Through dynamic spin-coating ($\sim 70 \mu\text{L}$, ~ 4000 rpm, 30 sec), a 35 nm thick SiQD layer was obtained. ZnO layer (25 nm) was also fabricated through dynamic spin-coating ($\sim 100 \mu\text{L}$, ~ 3000 rpm, 30 sec). Each layer was annealed at 140 °C for 10 min immediately after spin-coating. A 3x3 mm device area was defined via a shadow mask when depositing the Ag top electrodes (3 $\text{\AA} \text{ s}^{-1}$, $<10^{-5}$ mbar). The used Leybold Univex 350 PVD system was directly attached to the glovebox to avoid any material degradation. Finally, a thin glass slide was glued on top of the SiQD LED, using an Araldite 2011 two-component epoxy resin, for further protection.

SiQD-cLED Fabrication. Cavity LEDs with structure of glass/Ag/SiO₂/ITO/PEDOT:PSS/Poly-TPD/SiQDs/ZnO/Ag were fabricated on blank glass

substrates. All substrates were cleaned with acetone and isopropanol sonication baths, and subsequently blew dried with pressurized N₂ to remove solvent residues. The Ag output coupler and the SiO₂ spacer were then thermally or electron-beam evaporated onto the clean glass substrate. The ITO electrode (100 nm) was next sputtered onto the bottom layers via a patterned shadow mask. Next, the PEDOT:PSS, Poly-TPD, SiNCs, ZnO, and Ag top mirror electrode were fabricated using the same procedure as making the normal SiQD LED.

Fourier Transform Infrared Spectroscopy (FT-IR). FT-IR spectrum was acquired with a liquid nitrogen-cooled Bruker Vertex 70 A on an attenuated total reflection module and a resolution of 4 cm⁻¹. The spectrum was processed by the software Opus.

Thermal Gravimetric Analysis (TGA). TGA samples were prepared by freeze-drying SiQDs in benzene to obtain an orange powder. The measurement was carried out by a Netzsch TG 209 F 1 Libra inside a glovebox with the sample in an aluminum oxide pans. The heat rate was 10 °C min⁻¹ from 30 to 750 °C under an argon flow of 20 mL min⁻¹. The data was processed with the software Netzsch Proteus 6.

X-ray Photoelectron Spectroscopy (XPS). XPS samples were prepared by drop-casting benzene suspensions of the SiQDs on a copper foil. A Kratos Axis 165 Ultra X-ray photoelectron spectrometer was used to obtain survey and high-resolution spectra. A monochromatic Al K α source (140 W) with a set energy (1486.6 eV) was used to obtain the spectra. The electron takeoff angle for the spectra was 90°. The Si 2p spectra were calibrated to the aliphatic C 1s signal (284.8 eV) using CasaXP (VAMAS) software and using a Shirley-type background. To fit the Si 2p high-resolution spectrum to Si 2p_{3/2} and Si 2p_{1/2} components, the doublet area was fixed at a 2:1 ratio and separated by a spin-orbit splitting (0.61 eV). The spectra were fit using a symmetric Gaussian-Lorentzian line shape splitting into different energies.

Transmission Electron Microscopy (TEM). TEM samples were prepared by drop-casting benzene suspension of the SiQDs onto a lacey carbon grid and solvent was evaporated in a vacuum chamber. The bright-field TEM images were acquired using a JEOL-2012 electron microscope equipped with LaB6 filament and operated at an accelerating voltage of 200 kV. Particle size distribution was calculated by counting at least 300 particles using ImageJ software. The corresponding average shifted histogram (ASH) was plotted using a web-application accessed at the following url: <http://maverick.chem.ualberta.ca/plot/ash>.⁶⁰

Photoluminescence (PL) Characterization. Samples for the optical measurements were prepared by placing the SiQD benzene solution inside a quartz cuvette. The PL spectrum was recorded using an Avantes AvaSpec 2048 spectrometer coupled with a Prizmatix light source ($\lambda_{\text{ex}} = 365 \text{ nm}$) and processed with the software Avasoft 8. UV-Vis absorption spectrum was acquired by a Varian Cary 50 Scan spectrometer. The absolute quantum yield value was obtained using a Hamamatsu Absolute PL Quantum Yield C11347 spectrometer equipped with an integrated sphere. The measured values were calculated by the supplied software *via* Equation S1.

Reflectivity Characterization. The reflectance spectra of the Ag layers and cLEDs were measured by an AvaSpec 2048 spectrometer with a spectral range from 175 to 1300 nm. An AvaLight-DH-S-BAL ($\lambda = 215 - 2500 \text{ nm}$) was used as the excitation source, where the source and reflections was collected by a reflection probe positioned normal to the sample. The reflections of the Ag thin films were calibrated using a Thorlabs PF10-03-P01 mirror (Avg. reflectivity of ca. 97% at 700 nm); the cLED reflections were calibrated to a specimen coated with the 100 nm silver mirror.

Thin Film Characterizations. Profilometry measurements of LED layer thicknesses were measured over a thin cut on the reference films using a Bruker DektakXT stylus profilometer. The

ITO work function was measured by Kelvin probe KP020 from KP Technology. Atomic force microscopic images were recorded using Veeco Dimension Icon in tapping mode and analyzed with Gwyddion software. Refractive indices of the layers were collected a Woollam alpha-SE ellipsometer under angles of 65° , 70° , and 75° in the wavelength range from 380 nm to 900 nm. The data of ITO thin film was fitted with the Drude-Lorentz-model and the other active layers were fitted with the Cauchy-model.

Simulation of Reflection. The theoretical reflection spectra were simulated by TFCalc. The incident beam was set to be 700 nm wavelength illuminating with normal to the surface of the cavity. The substrate was set to be a 1.0 mm thick glass followed by cLED layers (e.g., Ag output coupler, SiO₂, ITO, PEDOT:PSS, etc.) added as front layers. The spectra were calculated using the experimental refractive indices of the materials meanwhile cavity thicknesses varied by SiO₂ thicknesses.

LED Characterizations. The electroluminescence spectra of the control SiQD-LED were collected by a calibrated AvaSpec-ULS2048 X 64 TEC spectrometer (Avantes) coupled with a Thorlabs IS200-4 integrating sphere. A two-channel Keithley 2602A source measure unit was used for characterizing the device's electronic properties. Coupled with the same AvaSpec spectrometer, the EL spectra of the cLED were collected with an optical fiber positioned at the normal. A two-channel Keithley 2636 source measure unit and a Thorlabs FDS10X10 photodiode were used for characterizing the devices opto-electronically. The measurements were controlled and analyzed with Matlab, where detailed calculation of EQE was shown in Equation S2-4.

Cavity Analysis. The simulated transmittance spectra of the SiQD-cLEDs were calculated by software TFCalc35 with the experimental refractive indices of the active layers. More detailed

calculations of the cavity FWHM, quality factor, and finesse can be found in the Supplementary Information.

ASSOCIATED CONTENT

Supporting Information.

The Supporting Information is available free of charge on the ACS Publication website.

FT-IR spectra, TGA and XP spectra of C₆-SiQDs. Reflectance spectra of Ag thin films. Work function and profilometry measurements of ITO layer. Refractive indices of the active layers. Optoelectronic characterizations and EL spectra analysis of normal SiQD-LED. Reflectance and EL spectra analysis of SiQD-cLEDs. Angle-dependent and voltage-dependent EL of 50-cLED. Optoelectronic characterizations of 50-cLED. Calculations for PL and external quantum efficiency, FWHM, FSR, Q-factor, and Finesse.

AUTHOR INFORMATION

Corresponding Authors

Markus Becherer – E-mail: markus.becherer@tum.de

Jonathan G. C. Veinot – E-mail: jveinot@ualberta.ca

ORCID

I Teng Cheong: 0000-0002-3584-9800

Josef Mock: 0000-0002-0252-8824

Maria Kallergi: 0000-0002-7224-6734

Elisabeth Groß: 0000-0003-2058-5328

Alkiviathes Meldrum: 0000-0001-7215-4023

Bernhard Rieger: 0000-0002-0023-884X

Markus Becherer: 0000-0002-1291-8877

Jonathan G. C. Veinot: 0000-0001-7511-510X

Notes

The authors declare no competing financial interests. The authors declare no conflict of interest.

ACKNOWLEDGMENT

I T.C. and J.M. contributed equally as joint first authors to this work. The authors acknowledge the continued generous funding from the ATUMS training program supported by NSERC CREATE (CREATE-463990-2015), the Deutsche Forschungsgemeinschaft (DFG, German Research Foundation, project number 245845833), the Natural Science and Engineering Research Council (NSERC Discovery Grant program; RGPIN-2015-03896), Alberta Innovates Strategic Projects program, as well as Future Energy System (FES) which is supported by the Canada First Research Excellence Fund (CFREF). The support of the Central Electronics and Information Technology Laboratory – ZEIT^{lab} is greatly acknowledged. We also would like to thank Ph.D. Carsten Peters and Professor Sevil Weinkauff for help with transmission electron microscopy measurements, Sarah Milliken and staff at the Nanofab of University of Alberta for their assistances with XPS acquisition, Sebastian Weishäupl for help with PL quantum yield measurement, Andreas Zeidler for Kelvin Probe measurements, and Matthias Golibrzuch for the help with the AFM measurements. Finally, we acknowledge the efforts of all the other authors who have contributed to this work.

REFERENCES

(1) Rossetti, R.; Nakahara, S.; Brus, L. E. Quantum size effects in the redox potentials, resonance Raman spectra, and electronic spectra of CdS crystallites in aqueous solution. *The Journal of Chemical Physics* **1983**, 79 (2), 1086-1088. DOI: 10.1063/1.445834.

- (2) Ke, W.; Kanatzidis, M. G. Prospects for low-toxicity lead-free perovskite solar cells. *Nat Commun* **2019**, *10* (1), 965. DOI: 10.1038/s41467-019-08918-3.
- (3) Xu, Q.; Cheong, I. T.; Meng, L.; Veinot, J. G. C.; Wang, X. Silicon Surface Passivation for Silicon-Colloidal Quantum Dot Heterojunction Photodetectors. *ACS Nano* **2021**, *15* (11), 18429-18436. DOI: 10.1021/acsnano.1c08002.
- (4) Medintz, I. L.; Uyeda, H. T.; Goldman, E. R.; Mattoussi, H. Quantum dot bioconjugates for imaging, labelling and sensing. *Nature Materials* **2005**, *4* (6), 435-446. DOI: 10.1038/nmat1390.
- (5) Zhu, Q.-B.; Li, B.; Yang, D.-D.; Liu, C.; Feng, S.; Chen, M.-L.; Sun, Y.; Tian, Y.-N.; Su, X.; Wang, X.-M.; et al. A flexible ultrasensitive optoelectronic sensor array for neuromorphic vision systems. *Nature Communications* **2021**, *12* (1), 1798. DOI: 10.1038/s41467-021-22047-w.
- (6) Xiao, F.-X.; Miao, J.; Liu, B. Layer-by-Layer Self-Assembly of CdS Quantum Dots/Graphene Nanosheets Hybrid Films for Photoelectrochemical and Photocatalytic Applications. *Journal of the American Chemical Society* **2014**, *136* (4), 1559-1569. DOI: 10.1021/ja411651e.
- (7) Yonemoto, D. T.; Papa, C. M.; Mongin, C.; Castellano, F. N. Thermally Activated Delayed Photoluminescence: Deterministic Control of Excited-State Decay. *J Am Chem Soc* **2020**, *142* (25), 10883-10893. DOI: 10.1021/jacs.0c03331.
- (8) Li, N.; Chen, X.; Wang, J.; Liang, X.; Ma, L.; Jing, X.; Chen, D.-L.; Li, Z. ZnSe Nanorods–CsSnCl₃ Perovskite Heterojunction Composite for Photocatalytic CO₂ Reduction. *ACS Nano* **2022**, *16* (2), 3332-3340. DOI: 10.1021/acsnano.1c11442.
- (9) Liu, Z.; Lin, C. H.; Hyun, B. R.; Sher, C. W.; Lv, Z.; Luo, B.; Jiang, F.; Wu, T.; Ho, C. H.; Kuo, H. C.; et al. Micro-light-emitting diodes with quantum dots in display technology. *Light Sci Appl* **2020**, *9*, 83. DOI: 10.1038/s41377-020-0268-1.

- (10) Shirasaki, Y.; Supran, G. J.; Bawendi, M. G.; Bulović, V. Emergence of colloidal quantum-dot light-emitting technologies. *Nature Photonics* **2012**, *7* (1), 13-23. DOI: 10.1038/nphoton.2012.328.
- (11) Dai, X.; Deng, Y.; Peng, X.; Jin, Y. Quantum-Dot Light-Emitting Diodes for Large-Area Displays: Towards the Dawn of Commercialization. *Adv Mater* **2017**, *29* (14). DOI: 10.1002/adma.201607022.
- (12) Choi, M. K.; Yang, J.; Hyeon, T.; Kim, D.-H. Flexible quantum dot light-emitting diodes for next-generation displays. *npj Flexible Electronics* **2018**, *2* (1). DOI: 10.1038/s41528-018-0023-3.
- (13) Yin, Y.; Hu, Z.; Ali, M. U.; Duan, M.; Gao, L.; Liu, M.; Peng, W.; Geng, J.; Pan, S.; Wu, Y.; et al. Full-Color Micro-LED Display with CsPbBr₃ Perovskite and CdSe Quantum Dots as Color Conversion Layers. *Advanced Materials Technologies* **2020**, *5* (8). DOI: 10.1002/admt.202000251.
- (14) Won, Y.-H.; Cho, O.; Kim, T.; Chung, D.-Y.; Kim, T.; Chung, H.; Jang, H.; Lee, J.; Kim, D.; Jang, E. Highly efficient and stable InP/ZnSe/ZnS quantum dot light-emitting diodes. *Nature* **2019**, *575* (7784), 634-638.
- (15) Garcia de Arquer, F. P.; Talapin, D. V.; Klimov, V. I.; Arakawa, Y.; Bayer, M.; Sargent, E. H. Semiconductor quantum dots: Technological progress and future challenges. *Science* **2021**, *373* (6555). DOI: 10.1126/science.aaz8541 From NLM PubMed-not-MEDLINE.
- (16) Das, A.; Snee, P. T. Synthetic Developments of Nontoxic Quantum Dots. *Chemphyschem* **2016**, *17* (5), 598-617. DOI: 10.1002/cphc.201500837.
- (17) Ivanov, S.; Zhuravsky, S.; Yukina, G.; Tomson, V.; Korolev, D.; Galagudza, M. In Vivo Toxicity of Intravenously Administered Silica and Silicon Nanoparticles. *Materials* **2012**, *5* (10), 1873-1889. DOI: 10.3390/ma5101873.

- (18) Cheng, K. Y.; Anthony, R.; Kortshagen, U. R.; Holmes, R. J. High-efficiency silicon nanocrystal light-emitting devices. *Nano Lett* **2011**, *11* (5), 1952-1956. DOI: 10.1021/nl2001692.
- (19) Zhao, S.; Liu, X.; Pi, X.; Yang, D. Light-emitting diodes based on colloidal silicon quantum dots. *Journal of Semiconductors* **2018**, *39* (6). DOI: 10.1088/1674-4926/39/6/061008.
- (20) Ghosh, B.; Yamada, H.; Chinnathambi, S.; Ozbilgin, I. N. G.; Shirahata, N. Inverted Device Architecture for Enhanced Performance of Flexible Silicon Quantum Dot Light-Emitting Diode. *J Phys Chem Lett* **2018**, *9* (18), 5400-5407. DOI: 10.1021/acs.jpcllett.8b02278.
- (21) Angi, A.; Loch, M.; Sinelnikov, R.; Veinot, J. G. C.; Becherer, M.; Lugli, P.; Rieger, B. The influence of surface functionalization methods on the performance of silicon nanocrystal LEDs. *Nanoscale* **2018**, *10* (22), 10337-10342. DOI: 10.1039/c7nr09525b.
- (22) Mock, J.; Groß, E.; Kloberg, M. J.; Rieger, B.; Becherer, M. Surface Engineering of Silicon Quantum Dots: Does the Ligand Length Impact the Optoelectronic Properties of Light-Emitting Diodes? *Advanced Photonics Research* **2021**, *2* (9). DOI: 10.1002/adpr.202100083.
- (23) Ono, T.; Xu, Y.; Sakata, T.; Saitow, K. I. Designing Efficient Si Quantum Dots and LEDs by Quantifying Ligand Effects. *ACS Appl Mater Interfaces* **2022**, *14* (1), 1373-1388. DOI: 10.1021/acsami.1c18779.
- (24) Veinot, J. G. Synthesis, surface functionalization, and properties of freestanding silicon nanocrystals. *Chem Commun (Camb)* **2006**, (40), 4160-4168. DOI: 10.1039/b607476f.
- (25) Milliken, S.; Thiessen, A. N.; Cheong, I. T.; O'Connor, K. M.; Li, Z.; Hooper, R. W.; Robidillo, C. J. T.; Veinot, J. G. C. "Turning the dials": controlling synthesis, structure, composition, and surface chemistry to tailor silicon nanoparticle properties. *Nanoscale* **2021**, *13* (39), 16379-16404. DOI: 10.1039/d1nr04701a.

- (26) Hohlein, I. M.; Angi, A.; Sinelnikov, R.; Veinot, J. G.; Rieger, B. Functionalization of hydride-terminated photoluminescent silicon nanocrystals with organolithium reagents. *Chemistry* **2015**, *21* (7), 2755-2758. DOI: 10.1002/chem.201405555.
- (27) Halimaoui, A.; Oules, C.; Bomchil, G.; Bsiesy, A.; Gaspard, F.; Herino, R.; Ligeon, M.; Muller, F. Electroluminescence in the visible range during anodic oxidation of porous silicon films. *Applied Physics Letters* **1991**, *59* (3), 304-306. DOI: 10.1063/1.105578.
- (28) Koshida, N.; Koyama, H. Visible electroluminescence from porous silicon. *Applied Physics Letters* **1992**, *60* (3), 347-349. DOI: 10.1063/1.106652.
- (29) Ligman, R. K.; Mangolini, L.; Kortshagen, U. R.; Campbell, S. A. Electroluminescence from surface oxidized silicon nanoparticles dispersed within a polymer matrix. *Applied Physics Letters* **2007**, *90* (6). DOI: 10.1063/1.2471662.
- (30) Photopoulos, P.; Nassiopoulou, A. G. Room- and low-temperature voltage tunable electroluminescence from a single layer of silicon quantum dots in between two thin SiO₂ layers. *Applied Physics Letters* **2000**, *77* (12). DOI: 10.1063/1.1290603.
- (31) Walters, R. J.; Bourianoff, G. I.; Atwater, H. A. Field-effect electroluminescence in silicon nanocrystals. *Nat Mater* **2005**, *4* (2), 143-146. DOI: 10.1038/nmat1307.
- (32) Puzzo, D. P.; Henderson, E. J.; Helander, M. G.; Wang, Z.; Ozin, G. A.; Lu, Z. Visible colloidal nanocrystal silicon light-emitting diode. *Nano Lett* **2011**, *11* (4), 1585-1590. DOI: 10.1021/nl1044583.
- (33) Mastronardi, M. L.; Henderson, E. J.; Puzzo, D. P.; Chang, Y.; Wang, Z. B.; Helander, M. G.; Jeong, J.; Kherani, N. P.; Lu, Z.; Ozin, G. A. Silicon nanocrystal OLEDs: effect of organic capping group on performance. *Small* **2012**, *8* (23), 3647-3654. DOI: 10.1002/sml.201201242.

- (34) Maier-Flaig, F.; Rinck, J.; Stephan, M.; Bocksrocker, T.; Bruns, M.; Kubel, C.; Powell, A. K.; Ozin, G. A.; Lemmer, U. Multicolor silicon light-emitting diodes (SiLEDs). *Nano Lett* **2013**, *13* (2), 475-480. DOI: 10.1021/nl3038689.
- (35) Liu, X.; Zhao, S.; Gu, W.; Zhang, Y.; Qiao, X.; Ni, Z.; Pi, X.; Yang, D. Light-Emitting Diodes Based on Colloidal Silicon Quantum Dots with Octyl and Phenylpropyl Ligands. *ACS Appl Mater Interfaces* **2018**, *10* (6), 5959-5966. DOI: 10.1021/acsami.7b16980.
- (36) Watanabe, J.; Yamada, H.; Sun, H.-T.; Moronaga, T.; Ishii, Y.; Shirahata, N. Silicon Quantum Dots for Light-Emitting Diodes Extending to the NIR-II Window. *ACS Applied Nano Materials* **2021**, *4* (11), 11651-11660. DOI: 10.1021/acsanm.1c02223.
- (37) Kveder, V.; Badylevich, M.; Steinman, E.; Izotov, A.; Seibt, M.; Schröter, W. Room-temperature silicon light-emitting diodes based on dislocation luminescence. *Applied Physics Letters* **2004**, *84* (12), 2106-2108. DOI: 10.1063/1.1689402.
- (38) Maier-Flaig, F.; Kubel, C.; Rinck, J.; Bocksrocker, T.; Scherer, T.; Prang, R.; Powell, A. K.; Ozin, G. A.; Lemmer, U. looking inside a working SiLED. *Nano Lett* **2013**, *13* (8), 3539-3545. DOI: 10.1021/nl400975u.
- (39) Yao, L.; Yu, T.; Ba, L.; Meng, H.; Fang, X.; Wang, Y.; Li, L.; Rong, X.; Wang, S.; Wang, X.; et al. Efficient silicon quantum dots light emitting diodes with an inverted device structure. *Journal of Materials Chemistry C* **2016**, *4* (4), 673-677. DOI: 10.1039/c5tc03064a.
- (40) Terada, S.; Ueda, H.; Ono, T.; Saitow, K.-i. Orange–Red Si Quantum Dot LEDs from Recycled Rice Husks. *ACS Sustainable Chemistry & Engineering* **2022**, *10* (5), 1765-1776. DOI: 10.1021/acssuschemeng.1c04985.
- (41) Zhang, Y. C.; Yu, Z. Y.; Xue, X. Y.; Wang, F. L.; Li, S.; Dai, X. Y.; Wu, L.; Zhang, S. Y.; Wang, S. Y.; Lu, M. High brightness silicon nanocrystal white light-emitting diode with luminance

of 2060 cd/m²). *Opt Express* **2021**, 29 (21), 34126-34134. DOI: 10.1364/OE.437737 From NLM PubMed-not-MEDLINE.

(42) Talapin, D. V.; Steckel, J. Quantum dot light-emitting devices. *MRS Bulletin* **2013**, 38 (9), 685-691. DOI: 10.1557/mrs.2013.204.

(43) Sychugov, I.; Juhasz, R.; Valenta, J.; Linnros, J. Narrow luminescence linewidth of a silicon quantum dot. *Phys Rev Lett* **2005**, 94 (8), 087405. DOI: 10.1103/PhysRevLett.94.087405.

(44) Sychugov, I.; Fucikova, A.; Pevere, F.; Yang, Z.; Veinot, J. G. C.; Linnros, J. Ultranarrow Luminescence Linewidth of Silicon Nanocrystals and Influence of Matrix. *ACS Photonics* **2014**, 1 (10), 998-1005. DOI: 10.1021/ph500221z.

(45) Mastronardi, M. L.; Maier-Flaig, F.; Faulkner, D.; Henderson, E. J.; Kubel, C.; Lemmer, U.; Ozin, G. A. Size-dependent absolute quantum yields for size-separated colloiddally-stable silicon nanocrystals. *Nano Lett* **2012**, 12 (1), 337-342. DOI: 10.1021/nl2036194 From NLM Medline.

(46) Mastronardi, M. L.; Hennrich, F.; Henderson, E. J.; Maier-Flaig, F.; Blum, C.; Reichenbach, J.; Lemmer, U.; Kubel, C.; Wang, D.; Kappes, M. M.; et al. Preparation of monodisperse silicon nanocrystals using density gradient ultracentrifugation. *J Am Chem Soc* **2011**, 133 (31), 11928-11931. DOI: 10.1021/ja204865t.

(47) Hodgson, N.; Weber, H. The Fabry Perot Resonator. Springer London, 1997; pp 137-162.

(48) Amans, D.; Callard, S.; Gagnaire, A.; Joseph, J.; Huisken, F.; Ledoux, G. Spectral and spatial narrowing of the emission of silicon nanocrystals in a microcavity. *Journal of Applied Physics* **2004**, 95 (9), 5010-5013. DOI: 10.1063/1.1669073.

(49) Hryciw, A.; Laforge, J.; Blois, C.; Glover, M.; Meldrum, A. Tunable Luminescence from a Silicon-Rich Oxide Microresonator. *Advanced Materials* **2005**, 17 (7), 845-849. DOI: 10.1002/adma.200401230.

- (50) Zeng, P.; Wang, F.; Zhang, Y.; Zhou, W.; Guo, Z.; Wu, X.; Lu, M.; Zhang, S. Edge-Emitting Silicon Nanocrystal Distributed Feedback Laser with Extremely Low Exciton Threshold. *ACS Photonics* **2021**, *8* (5), 1353-1363. DOI: 10.1021/acsp Photonics.0c01846.
- (51) Zhang, Y.-C.; Yu, Z.-Y.; Ma, F.-Y.; Xue, X.-Y.; Liu, K.-X.; Sun, J.; Wang, S.-Y.; Lu, M. Observation of distributed feedback lasing in silicon nanocrystals under electrical pumping. *Results in Physics* **2022**, *39*. DOI: 10.1016/j.rinp.2022.105734.
- (52) Cheong, I. T.; Morrish, W.; Sheard, W.; Yu, H.; Tavares Luppi, B.; Milburn, L.; Meldrum, A.; Veinot, J. G. C. Silicon Quantum Dot-Polymer Fabry-Perot Resonators with Narrowed and Tunable Emissions. *ACS Appl Mater Interfaces* **2021**, *13* (23), 27149-27158. DOI: 10.1021/acсами.1c01825.
- (53) Yang, Z.; Iqbal, M.; Dobbie, A. R.; Veinot, J. G. Surface-induced alkene oligomerization: does thermal hydrosilylation really lead to monolayer protected silicon nanocrystals? *J Am Chem Soc* **2013**, *135* (46), 17595-17601. DOI: 10.1021/ja409657y.
- (54) Cheng, K.-Y.; Anthony, R.; Kortshagen, U. R.; Holmes, R. J. Hybrid Silicon Nanocrystal–Organic Light-Emitting Devices for Infrared Electroluminescence. *Nano Letters* **2010**, *10* (4), 1154-1157. DOI: 10.1021/nl903212y.
- (55) Mock, J.; Kallergi, M.; Gro, E.; Golibrzuch, M.; Rieger, B.; Becherer, M. Revealing the Negative Capacitance Effect in Silicon Quantum Dot Light-Emitting Diodes Via Temperature-Dependent Capacitance-Voltage Characterization. *IEEE Photonics Journal* **2022**, 1-10. DOI: 10.1109/jphot.2022.3184401.
- (56) Ma, F.; Liu, X. Phase shift and penetration depth of metal mirrors in a microcavity structure. *Appl. Opt.* **2007**, *46* (25), 6247-6250. DOI: 10.1364/AO.46.006247.

- (57) Weiss, E. A. Designing the Surfaces of Semiconductor Quantum Dots for Colloidal Photocatalysis. *ACS Energy Letters* **2017**, *2* (5), 1005-1013. DOI: 10.1021/acsenergylett.7b00061.
- (58) Chen, J.; Wang, Z.; Chen, Z.; Cong, S.; Zhao, Z. Fabry-Perot Cavity-Type Electrochromic Supercapacitors with Exceptionally Versatile Color Tunability. *Nano Lett* **2020**, *20* (3), 1915-1922. DOI: 10.1021/acs.nanolett.9b05152.
- (59) Wang, Z.; Wang, X.; Cong, S.; Chen, J.; Sun, H.; Chen, Z.; Song, G.; Geng, F.; Chen, Q.; Zhao, Z. Towards full-colour tunability of inorganic electrochromic devices using ultracompact fabry-perot nanocavities. *Nat Commun* **2020**, *11* (1), 302. DOI: 10.1038/s41467-019-14194-y.
- (60) Anderson, S. L.; Lubber, E. J.; Olsen, B. C.; Buriak, J. M. Substance over Subjectivity: Moving beyond the Histogram. *Chemistry of Materials* **2016**, *28* (17), 5973-5975. DOI: 10.1021/acs.chemmater.6b03430.